Interplay between Charge and Magnetic Orderings in YbPd

Atsushi MIYAKE[1][*][†], Kazuki KASANO[1], Tomoko KAGAYAMA[1], Katsuya SHIMIZU[1],
Ryo TAKAHASHI[2], Yusuke WAKABAYASHI[2], Tsuyoshi KIMURA[2] and Takao EBIHARA[3]

[1]*KYOKUGEN, Osaka University, Toyonaka 560-8531, Japan,*
[2]*Graduate School of Engineering Science, Osaka University, Toyonaka 560-8531, Japan,*
[3]*Department of physics, Shizuoka University, Shizuoka 422-8529, Japan*

The pressure-temperature phase diagram of an intermediate-valence compound YbPd was revealed via simultaneous ac-calorimetry and electrical resistivity measurements. Two successive structural phase transition temperatures, $T_1 = 125$ K and $T_2 = 110$ K, are found to decrease with increasing pressure. The magnetic ordering transition at $T_N \sim 1.9$ K decreases monotonically up to 1.7 GPa and disappears discontinuously at $P_c \sim 1.9$ GPa, where the structural phase transition at T_2 is also suppressed. At P_c, enhancement of the effective mass and residual resistivity are observed. Another probable magnetic phase transition, however, is found to take place at $T_{ML} \sim 0.3$ K and smoothly varies even when crossing P_c. Structural phase transitions at ambient pressure were also studied by a single crystal X-ray diffraction measurement. Below T_2, a tetragonal lattice distortion with doubling of the unit cell along the c-axis is observed, and thus there are two inequivalent Yb-sites below P_c. These results indicate that one Yb-site, having larger valence configuration and thus smaller Kondo temperature, orders at T_N. The other phase transition at T_{ML} seems to couple to the crystal structure for $T_2 < T < T_1$. YbPd is a unique system exhibiting magnetic orderings in metallic charge-ordered Yb systems.

KEYWORDS: YbPd, charge ordering, magnetic ordering, pressure-temperature phase diagram

1. Introduction

Various novel ground states of many Ce and Yb based intermetallic compounds have been considerably studied.[1,2] Unconventional superconductivity and deviation from Fermi liquid behavior due to the enhancement of quantum fluctuations at the quantum critical point have been observed, for example, in CeIn$_3$ and β-YbAlB$_4$.[3,4] When the doublet ground state in these Kramers ions is realized, the exchange interaction between the conduction electrons and f-electrons seems to determine the ground state. The Ruderman-Kittel-Kasuya-Yosida interaction stabilizes the magnetic ground state, while the screening of the magnetic moment occurs due to the formation of the Kondo singlet. For Ce systems, the magnetic ordered state is suppressed under pressure, which has often been compared with Doniach's phase diagram.[5] Yb-based compounds with a Yb^{3+} configuration, one $4f$ hole, are thought to be countersystems to the one $4f$ electron of trivalent Ce-systems. In contrast to Ce systems, pressure-induced magnetic phase transitions are often observed in Yb-systems.

The differences between Ce and Yb systems have recently been discussed.[6,7] Because of the different hierarchies of the energy scales, such as Kondo temperature, $4f$-band width, and crystal electric fields, in the real lattice Yb-valence varies widely between the non-magnetic

$2 + (J = 0)$ and the magnetic $3 + (J = 7/2)$, while Ce valence varies only between $3 + (J = 5/2)$ and $\sim 3.2+$. In the former case of intermediate valence, the Kondo temperature T_K could be small due to the narrower $4f$-band than Ce. Thus Yb-compounds are expected to have a magnetic and/or heavy fermion state even in the valence fluctuating regime, something which is only realized in the very nearly trivalent configuration for Ce-systems.

Another intriguing phenomenon is charge ordering; Yb^{3+} and Yb^{2+}-configurations lie on the sublattices, for example, in semimetallic Yb$_4$As$_3$.[8] In contrast, for metallic cases hybridization between $4f$ and conduction electrons may lead to charge orderings of different non-integer configurations. Being distinguished from the homogeneous intermediate valence systems, such materials are called heterogeneous mixed-valence systems. These compounds have two or more crystallographically inequivalent sites, and the valences for the respective sites are different. Because of their different electronic configurations, magnetic ordering may occur for one of the sublattices. However, the magnetically ordered state is rarely observed in heterogeneous mixed valence systems.

YbPd has been suggested as one such metallic heterogeneous mixed-valence system and shows puzzling four phase transitions at 125, 110, 1.9 and 0.5 K, although it crystallizes in a simple CsCl-structure under ambient conditions.[9,10] The higher temperature transitions at $T_1(T_2) = 125$ K (110 K) have been detected as symmetric sharp peaks in the temperature depen-

dences of thermal expansion coefficient and specific heat, and a clear thermal hysteresis in the electrical resistivity.[9, 12] However, no anomalies in the magnetic susceptibility have been reported, implying first-order structural phase transitions.[11, 12] Its structural distortion has been revealed by Raman scattering experiments; the crystal structure of YbPd loses four-fold symmetry at 4 K, and appears to begin to deform below T_1=125 K.[13] At $T_N \sim$ 1.9 K, an antiferromagnetic phase transition has been confirmed via magnetic susceptibility and Mössbauer measurements.[9, 10] In contrast to the other Yb-compounds, in which pressure often stabilizes the magnetic ground state, the pressure suppression of T_N in YbPd is manifested by a negative thermal expansion coefficient jump.[9, 14] In fact, it has been reported that T_N decreases with increasing pressure.[15] In addition, the susceptibility and the thermal expansion show clear thermal hysteresis around $\sim$0.5 K.[9, 14] Despite many experimental works in the literature, the origin of the phase transition has not yet been solved.

Moreover, it has been indicated by Mössbauer studies that the non-magnetic and magnetic Yb-sites coexist in almost equal proportions in the ordered state.[10] The magnetization and magnetic entropy are well reproduced by assuming that half of the Yb-ions have the magnetic Yb^{3+} configuration.[12, 14] Therefore, it is proposed that half of the Yb-ions form a heavy fermion antiferromagnet and that the structural phase transitions at T_1 and T_2 are associated with ordering of the Yb-valence, i.e., the magnetic state close to Yb^{3+} and the nonmagnetic one having intermediate valence.[10, 14, 15] However, there is no experimental evidence of charge ordering in YbPd, such as the the existence of a detailed pressure-temperature phase diagram including the low temperature region and the observation of crystallographic inequivalent Yb-sites.

In this paper, we have carefully determined the pressure-temperature phase diagram via precise electrical resistivity and ac-calorimetry measurements. On the basis of these measurements, we discuss the interplay between the valence and magnetic instabilities in YbPd. The magnetic phase below T_N only exists up to $P_c \sim$ 1.9 GPa, where the phase transition at T_2 is also suppressed, while another probable magnetic phase transition at $T_{ML} < T_N$ still remains across P_c. Tetragonal lattice distortion below T_2 is observed via single crystal X-ray diffraction measurements at ambient pressure, indicating the existence of the two inequivalent crystallographic Yb-sites. Because of the resultant different surroundings of Yb-ions, different characteristic energies, namely T_K varying with $4f$-occupation number, cause one of the Yb-sites to magnetic order at T_N. The other magnetic phase transition at T_{ML} seems to couple to the structure for $T_2 < T < T_1$. Possible scenarios explaining the low temperature magnetism in this heterogeneous mixed-valence system are discussed.

2. Experimental

Single crystals of YbPd were grown by the self flux method.[16] Typical dimensions of the grown crystals were $1\times1\times1$ mm^3. A CuBe diamond-anvil pressure cell filled with glycerin as a pressure-transmitting medium was used for applying pressure. The pressure was changed at room temperature and determined by a ruby fluorescence method at 10 K. The pressure medium remained liquid up to $\sim$5 GPa and at room temperature,[17, 18] indicating that hydrostatic conditions were well satisfied in the studied pressure range. For simultaneous electrical resistivity ρ and ac-calorimetry C_{ac} measurements, two Au-Au<u>Fe</u>(0.07%) thermocouples (TC) and two gold wires were welded on the edges of a rectangular shaped sample with a size of $\sim 200~\mu$m$\times80~\mu$m$\times40~\mu$m. ρ was measured by the four probe ac method down to 60 mK. For C_{ac} measurements, the sample temperature was modulated by the ac current through the sample between 60 mK and 4 K. The suitable modulating frequency was usually determined by the frequency dependence of lock-in-voltage A, as shown in Fig.1. At 0.3 K, non trivial dispersion of A around $\omega \sim$10 Hz was seen, and it was suppressed at 0.07 K. As a result, the measuring frequency in this work was fixed at $\omega = 203$ Hz, which is well above the frequency showing anomaly in $A(\omega)$ below 0.5 K and satisfies the measuring condition. Taking into account the phase shift between heater and TC, ϕ, we calculate C_{ac} using the formula; $C_{ac} = -P_0 \sin\phi/\omega|T_{ac}|$, where P_0 is the heating power. The relative change of C_{ac} as a function of pressure above T_N were directly comparable, because the same modulation current and frequency, and the same experimental electronics were used for each pressure.

Single crystal X-ray diffraction measurements were performed with a four-circle X-ray diffractometer attached to a rotating anode Mo K_α X-ray generator at ambient pressure. The sample temperature was controlled using a closed cycle refrigerator.

3. Experimental results

3.1 Pressure dependence of T_1 and T_2

First, we address the pressure dependence of the high temperature structural phase transitions at T_1 and T_2 as observed from electrical resistivity measurement. Fig. 2(a) represents the temperature dependence of the resistivity $\rho(T)$ at several pressures. In the high temperature region above T_1, $\rho(T)$ is insensitive to temperature but drops at T_1 and T_2 on cooling. These drops are clearly seen as peaks in the dρ/dT curves in Fig. 2(b). T_1 and T_2 are observed to decrease with increasing pressure. This behavior is in agreement with previously reported resistivity and thermal expansion measurements for polycrystalline samples.[12, 15] A broad peak corresponding to dρ/dT of around 16 K is also observed and is insensitive to pressure. A similar anomaly has been exhib-
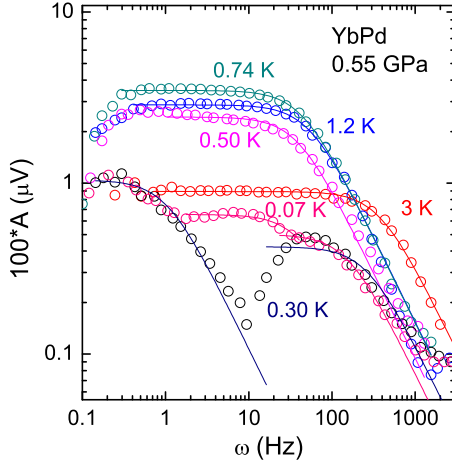
Fig. 1. (Color online) Frequency dependence of Lock-in-voltage A, which is proportional to T_{ac}, at 0.55 GPa and several temperatures. The lines show fitting results for the equation $A \propto T_{ac} = P_0/(\kappa + i\omega C)$, where κ is the thermal conductivity between sample and the environment. For ac-calorimetry measurements, $\omega > \kappa/C$ should be satisfied. Note that a dispersion $A(\omega)$ appears below $T_{MH} \sim 0.5$ K, probably reflecting phase separation or the coexistence of higher and lower temperature phases.

Fig. 2. (Color online) Temperature dependences of (a)ρ and (b) the temperature derivative $d\rho/dT$ of YbPd under different pressures. The arrows indicate the structural transition temperatures T_1 and T_2.

ited in the specific heat measurements,[9] although its origin is not clear. Above 1.74 GPa, T_2 is suppressed. Interestingly, at low temperature ρ is strongly enhanced; this enhancement will be discussed later. Due to smearing of the $d\rho/dT$ anomaly at T_1 with increasing pressure, $T_1(P)$ can not be unambiguously determined above 2 GPa. However, previously reported thermal expansion measurements clearly detected the transition at T_1 at up to 1.7 GPa, implying it still exists at higher pressure.[15] T_1 may become 0 K at a pressure of ~ 4 GPa by linear extrapolation, which agrees with previous report.[15] These results suggest that the ground state changes while crossing these pressures, accompanied by deformation of the crystal structures for $T < T_2$, $T_2 < T < T_1$ and $T > T_1$, an important finding.

3.2 Pressure dependence of magnetic transitions

Precise simultaneous resistivity and ac-calorimetry measurements revealed the rich magnetic pressure-temperature phase diagram of YbPd. Figures 3 (a) and (b) represent the temperature dependence of the resistivity ρ and the ac specific heat divided by temperature C_{ac}/T under several pressures and below 2.5 K. At the lowest measured pressure of $P \sim 0.25$ GPa, a kink in ρ and a λ-shaped anomaly in C_{ac}/T appear at $T_N \sim 1.9$ K. This temperature is in agreement with previous reports.[9,14] On further cooling, a drop in ρ and a peak in C_{ac}/T are observed at 0.47 K, also as previously reported.[14] This temperature is hereafter labeled T_{MH}. The transition at T_{MH} is obviously first order, due to the observation of thermal hysteresis. The first order
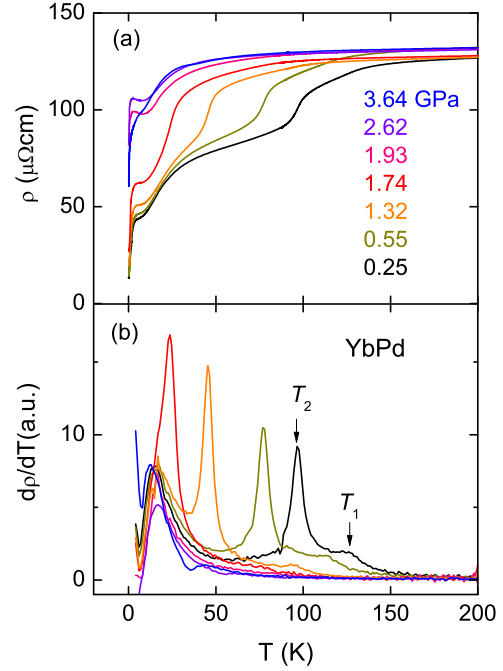
phase transition at T_{MH} may be a transition between two magnetic structures, such as a transition between incommensurate and commensurate. The dispersion of $A(\omega)$ below 0.5 K in Fig. 1 may relate to this first order phase transition. Surprisingly, another peak appears in C_{ac}/T at ~ 0.30 K, while no anomaly in $\rho(T)$ is observed. While two similar peaks in the susceptibility at 0.3 K and 0.7 K on warming have previously been reported,[9] the authors did not declare whether the anomaly corresponded to the phase transition. We confirm the existence of a phase transition thermodynamically, and the transition temperature is hereafter labeled as T_{ML}. Because of the doublet ground state, the phase transition at T_{ML} is magnetic in origin. This will be discussed in detail later. Thus, in addition to the known four phase transitions, we have newly found a magnetic phase transition.

With increasing pressure, T_N decreases monotonically, T_{MH} increases with suppression of the hysteresis loop, and T_{ML} weakly increases. The hysteresis loop around T_{MH} closes at $P \sim 1.45$ GPa and $T \sim 0.72$ K. T_{MH} disappears as if the first order transition has changed to a crossover. Above 1.9 GPa, any anomalies corresponding to the phase transition at T_N are not observed, indicating that the transition is suppressed discontinuously. Moreover, both $\rho(T)$ and $C_{ac}(T)/T$ curves are drastically changed and their values are enhanced, as shown in Fig. 3. At 1.93 GPa, $C_{ac}(T)/T$ only shows a
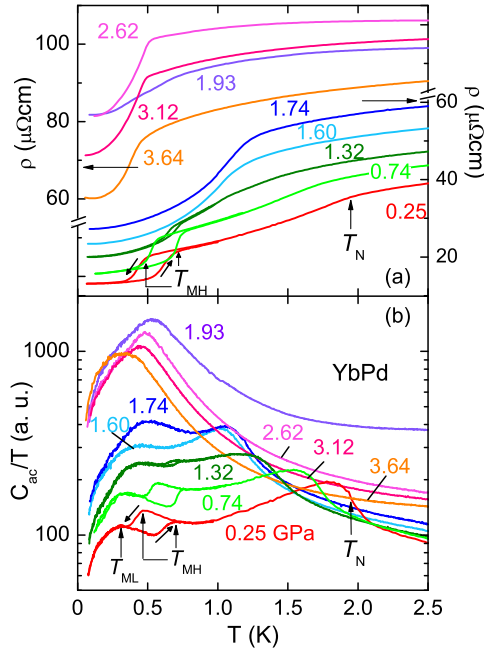
Fig. 3. (Color online) Temperature dependences of (a) ρ and (b) C_{ac}/T (semi-log plot) of YbPd under different pressures. The right and left scales in (a) are for below and above 1.74 GPa, respectively. The arrows indicate T_N, T_{MH}, and T_{ML}. The thermal hysteresis around T_{MH} for $P < P_{cr} \sim 1.45$ GPa is also notable.
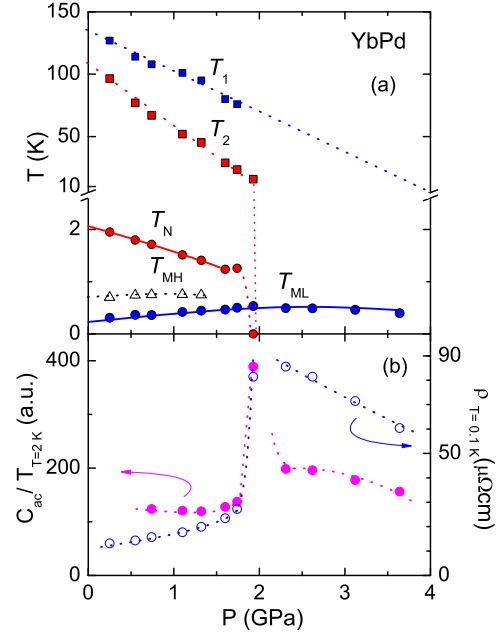

Fig. 4. (Color Online) (a) Pressure temperature phase diagram of YbPd. T_1, T_2, and T_{MH} on warming are plotted. (b) Pressure dependence of the C_{ac}/T in the paramagnetic phase of T = 2 K (left scale) and ρ at 0.1 K (right scale).

broad peak at ~ 0.6 K, and a broad kink in $\rho(T)$ is observed correspondingly. At higher pressure this broad kink in $\rho(T)$ is more pronounced. The temperature connects to T_{ML} at lower pressure, implying that the anomalies correspond to the phase transition at T_{ML}. Finally, T_{ML} varies smoothly with pressure, while T_N disappears around 1.9 GPa.

3.3 Pressure-temperature phase diagram

The pressure-temperature phase diagram of YbPd is depicted in Fig 4 (a). With increasing pressure, T_1, T_2, and T_N decrease, while T_{MH} and T_{ML} increase. The hysteresis and anomalies in $C_{ac}(T)/T$ and $\rho(T)$ at T_{MH} disappear above 1.5 GPa. These results suggest that the probable magnetic phase transition changes to a crossover. Interestingly, the magnetic ordering at T_N couples strongly to the structural phase transition at T_2. T_N is suppressed discontinuously at $P_c \sim 1.9$ GPa, where the transition at T_2 also collapses, as seen in Fig. 2. These results mean that P_c is first order in nature. T_N only exists below T_2.

As shown in Fig. 4 (b), the effective mass deduced by C_{ac}/T at $T = 2$ K in the paramagnetic state shows a sharp peak. Here, the mass enhancement seems to be driven by the change in crystal structure and the collapse of magnetism. In the case of CeIn$_3$, mass enhancement is observed at 2.5 GPa,[19] where the antiferromagnetism

collapses discontinuously.[20] Similarly, for YbPd the small energy of $T_N \sim 1.2$ K seems to give rise to a significant fluctuation and thus mass enhancement even at the first order critical point. In addition, ρ at 0.1 K, approximately the residual resistivity, is strongly enhanced across P_c. This may be due to the change in crystal structure and the resultant valence. Theoretically, it is proposed that the enhancement of residual resistivity occurs at the critical point or even crossover of the valence change.[21] These characteristics suggest that the charge ordering occurs at T_2 and is suppressed at P_c. At ambient pressure, however, the averaged Yb-valence of YbPd is $\sim 2.8+$ and is insensitive to temperature even when crossing T_1 and T_2. Therefore, the structural phase transitions at T_1 and/or T_2 are expected to make the Yb-sites inequivalent.

3.4 X-ray diffraction measurements using single crystal

The cubic structure observed at room temperature changes to a tetragonal structure at low temperature.[10] Moreover, Raman scattering measurements revealed that the symmetry of the crystal structure at 4 K is lower than the tetragonal symmetry.[13] To address the structural phase transitions at T_1 and T_2 in more detail, we performed X-ray diffraction measurements using an as-grown single crystal at ambient pressure. Here, the preliminary results explaining the phase diagram are presented, while the details will be reported elsewhere.[22]

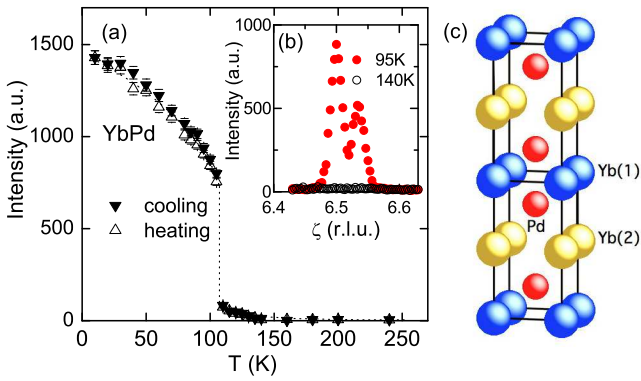Splitting of the Bragg reflection at $Q_B = (0, 0, l)$,

Fig. 5. (Color online) (a) Temperature dependence of the super-lattice reflection intensity at $Q_s = (0, 0, 6.5)$ at ambient pressure. The full and open symbols indicate data obtained on cooling and heating, respectively. (b) Superlattice peak profiles along the $(0\ 0\ \zeta)$ line measured at 140 K (above T_1) and 95 K (below T_2). The peak splitting is due to the Mo $K\alpha_1$ and $K\alpha_2$. (c) The most probable structural model for LT-phase ($T < T_2$). The unit cell is doubled along the c-axis due to the displacement of Pd-atoms. The distance of Yb(1)-Pd is shorter than that of Yb(2)-Pd.

where l is an integer, was clearly observed below T_1 (not shown), indicating that the symmetry below T_1 is lower than cubic. Moreover, an intense superlattice reflection at $Q_s = (0,\ 0,\ 6.5)$ was observed below T_2 as shown in Fig. 5(b). The superlattice reflection intensity discontinuously appears at T_2 and increases on further cooling, confirming a first order nature (Fig. 5(a)). No other superlattice reflections are observed at either $(n/2\ n/2\ n/2)$ or $(n/2\ n/2\ 0)$. These results indicate that below T_2 the crystal structure is tetragonal with a doubled unit cell along the c-axis. At 10 K, the c/a ratio is approximately 1.007, in good agreement with the previously reported value.[10] The most probable structure model below T_2 is that the Pd atoms displace along the c-axis, resulting in the two inequivalent Yb-sites, as shown in Fig. 5(c). The Yb-sites with shorter and longer distances to Pd are labeled as Yb(1) and Yb(2), respectively. The valence of the Yb(1)-ion is expected to be larger than that of Yb(2), because the radius of the Yb^{3+} ion is smaller than that of Yb^{2+}. Below P_c, the Yb(1) sublattice seems to order magnetically.

In this study, we could not observe any breaking of the four-fold symmetry as reported from the Raman scattering measurements.[13] It is important to reveal whether the four-fold symmetry is preserved at lower temperature. In any case, two inequivalent Yb-sites exist below T_2.

4. Discussion

The charge ordering of YbPd has been proposed as the ordering of magnetic and non-magnetic Yb-ions in almost equal quantities at 50 mK.[10] Here, we have revealed that the structural phase transition from cubic to tetragonal symmetry at T_2 causes the Yb-sites to exist as two inequivalent ones, as shown in Fig. 5(c). It is expected that the electronic configurations of Yb(1) and Yb(2) are different. This phase transition is reminiscent of the charge ordering observed in Yb_4As_3.[8] The ordering is also accompanied by the structural phase transition from cubic to trigonal symmetry.[24] In the charge ordered state, there are two inequivalent Yb-sites; 1/4 of the Yb-ions exist as Yb^{3+} arraed along the [1 1 1]-direction and the other 3/4 Yb-ions in the unit cell are Yb^{2+}.[25] The mean Yb-valence is thus expected to ~2.25+ from the ratio of the divalent and trivalent Yb-ions, which is in good agreement with the effective moment.[8] In contrast to metallic YbPd, Yb_4As_3 is a semi-metal having an extremely low carrier concentration of 0.001 per Yb-atom.[8] A difference between high and low carrier systems appears in their resistive anomaly at charge ordering temperature. The latter exhibits a sudden increase in the resistivity because the charge ordering decreases the carrier density. In contrast, for YbPd the resistivity decreases at T_1 and T_2, as shown in Fig. 2(a). The carrier density is almost constant, because the average valence is insensitive to temperature, and the decrease in resistivity arises from the suppression of valence fluctuation.

For YbPd, the average valence is ~2.8 and is insensitive to temperature. Therefore, charge ordering of the divalent and trivalent configurations in equal proportions is ruled out. It is expected that the charge is screened through the hybridization between conduction and f electrons (c-f hybridization), and thus the intermediate valence state may be stabilized in such metallic systems. Some Yb compounds, for example $Yb_2Pt_3Sn_5$[26] and Yb_5Si_3,[27] and $YbPd_3S_4$,[28] are known to be heterogeneous mixed-valence systems. In stark contrast to the semiconducting Yb_4As_3, for metallic systems the intermediate valence of the Yb-ions lie on the ordered sublattices. The interesting and remarkable phenomena exhibited by YbPd compared to these heterogeneous mixed-valence systems are the magnetic orderings in the charge ordered phases, and that they can be tuned by altering the external pressure. This is due to the moderate balance between charge and spin screenings through the c-f hybridization.

The Yb^{3+}-ion in the non-cubic lattice splits the $J = 7/2$ multiplet into four Kramers doublets for YbPd below T_2. For the doublet ground state in zero applied field, magnetic ordered or heavy fermion states could be realized to lift the degeneracy in the case for $\Delta_{CEF} > k_B T_K$, where Δ_{CEF} is the splitting energy between ground and first excited states.[6,7] For YbPd, the observation of CEF inelastic scattering indicates T_K is comparable to Δ_{CEF}.[23] It is also known that T_K varies

with the occupation number of the $4f$ level n_f,

$$k_B T_K \sim \frac{(1 - n_f)}{n_f} \Delta_{4f} N_f, \qquad (1)$$

where Δ_{4f} and N_f are the $4f$-band width and the degeneracy of the $4f$ multiplet, respectively.[29–31] Owing to the much smaller Δ_{4f} of Yb than Ce, T_K could be smaller or comparable to Δ_{CEF} even in the intermediate-valence state ($n_f \ll 1$), which is in strong contrast to the Ce-case. This leads to intermediate valence Yb-systems in the magnetic ordering or paramagnetic heavy fermion states, which are usually restricted to the trivalent ($n_f = 1$) configuration in Ce.

The tetragonal distortion at T_2 excludes the proposed Γ_8 quartet ground state, and thus the possibility of quadrupolar ordering.[9, 23] Therefore, magnetic ordering is most probable at both T_N and T_{ML}. Yb(1), which has the shorter distance to Pd, is expected to have the larger valence due to the smaller ionic radius of Yb^{3+} than that of Yb^{2+}, and the resultant smaller T_K expected from Eq. (1). Conversely, Yb(2) has larger T_K. The different T_Ks seem to give rise to the different magnetic ordering transition temperatures for Yb(1)- and Yb(2)-sublattices, i.e. T_N and T_{ML}. From the above consideration, both transitions would be expected to disappear at P_c, where T_2 is suppressed. In fact, while T_N only exists below T_2, the phase transition at T_{ML} still remains above P_c. Thus, the T_{ML} transition seems to couple to the T_1 phase transition. These results indicate that charge orderings near and far from the trivalent configurations occur not only at T_2 but also at T_1.

While the existence of the phase transition at T_{ML} has been clearly observed both from the present ac-calorimetry results and previous susceptibility studies,[9] it could not be detected at ambient pressure in some experiments. The hyperfine field is not significantly changed at either T_{MH} or T_{ML}.[10] The resistivity also shows no anomaly at T_{ML} below P_c, as seen in Fig.3(b). The change in the magnetic scattering, probably in proportion to the change in the ordered moment, is very small. This may be in agreement with the lack of an anomaly in the hyperfine field; the experimental resolution for ^{140}Yb isotope Mössbauer has been reported to be 0.15 μ_B.[32] It may also be in agreement with the low transition temperature of $T_{ML} \sim$0.3 K. The ordered moment is significantly reduced through the c-f hybridization. In addition, the specific heat and thermal expansion results measured for a polycrystalline sample exhibited anomalies corresponding to the phase transition at T_N and T_{MH}, but not at T_{ML}.[14] Because the phase transition at T_{ML} couples with the crystal structure for $T_2 < T < T_1$, the polycrystalline crystal averages subtle sublattices, and thus the magnetic ordering at T_{ML} is smeared out. In addition, below P_c, the magnetic phase transition at T_N seems to smear the transition at T_{ML}. Across P_c, the anomalies in $\rho(T)$ and $C_{ac}(T)/T$ that correspond to the transition are significantly emphasized. The clear anomaly in $\rho(T)$ above P_c is due to the release of the large residual entropy. The existence of an interplay between T_1 and T_{ML} is further speculated from these results. We have also observed splitting of the Bragg peaks (not shown) and a small but significant development of the superlattice reflection below T_1 (Fig. 5(a)). Similarly to the structure observed below T_2, some of the Yb-ions have near trivalent configurations in the structure below T_1, and the sublattice is expected to order below T_{ML}.

At P_c, the effective mass (C_{ac}/T) and the residual resistivity are strongly enhanced. After peaking, the mass still remains at a larger value than that below P_c. This indicates that the magnetically ordered $4f$ electrons form heavy fermion states through hybridization with the conduction electrons. The enhancement of the residual resistivity at P_c indicates that the structure and the resultant valence change across P_c.[21] A similar enhancement in $\rho_0(P)$ at P_c has also been observed in YbInCu$_4$, which shows isostructural phase transition accompanying the first order valence transition at ambient pressure.[33] These results support the proposed scenario for the charge ordering of YbPd at T_1 and T_2; trivalent and the intermediate valence states lie on the sublattices. It is important to solve the crystal structure for $T_2 < T < T_1$, which is currently in progress.[22] It is also very important in revealing whether the ordered phase collapses at the pressure suppressing T_1.

Pressure often stabilizes the magnetic ground state in Yb-systems because Yb^{3+} has a smaller ionic radius than non-magnetic Yb^{2+}. In contrast, for YbPd the magnetic phases are suppressed with pressure as for the Ce Kondo lattices. The pressure dependence of Kondo temperature T_K and the antiferromagnetic exchange J for Ce- and Yb-based Kondo lattices have been discussed theoretically.[34] With increasing pressure, both T_K and J show a broad minimum in the case of Yb, while for Ce they increase monotonously. YbPd may locate near the pressure of the broad minimum in T_K and J in terms of Ref. 34. Moreover, the antiferromagnetic phase is destabilized with suppression of the low temperature phase. The charge ordering thus plays a very important role in the low temperature magnetism.

It is also interesting how the ground state varies above the expected critical pressure, where T_1 collapses. Above this pressure, the intermediate valence state is stabilized over the whole temperature range in a similar case to that of homogeneous valence fluctuating systems. The latter materials, for example YbCu$_2$Si$_2$, change ground state from non-magnetic to magnetic at relatively high pressure.[35] However, no pressure-induced phase transitions have been observed for YbPd at up to 8 GPa,.[15]

5. Conclusion

Precise electrical resistivity and ac-calorimetry measurements have revealed the unique pressure-temperature phase diagram of YbPd. In addition to the reported four phase transitions, we have found a lower temperature magnetic phase transition at $T_{\mathrm{ML}} \sim 0.3$ K. Single crystal X-ray diffraction measurements confirmed that the structural phase transition at T_2 doubles the unit cell along the c-axis, resulting in two inequivalent Yb-sites in the tetragonal symmetry. These results are decisive evidence of charge ordering in the metallic systems. One Yb-site having larger valence and smaller Kondo temperature may order magnetically at T_{N}. This scenario agrees with the fact that T_{N} is discontinuously suppressed at P_{c}, where T_2 collapses. In addition, strong enhancements of the residual resistivity and effective mass are observed at P_{c}, suggesting the development of spin and valence fluctuations. YbPd is a unique system which shows magnetic ordering in charge ordered states.

Acknowledgements

1) J. Flouquet: in *Progress in Low Temperature Physics*, ed. W. P. Halperin (Elsevier, Amsterdam, 2005) Vol. 15, p.139.
2) H. v. Lōhneysen, A. Rosch, M. Vojta and P. Wōlfle: Rev. Mod. Phys. **79** (2007) 1015.
3) N. D. Mathur, F. M. Grosche, S. R. Julian, I. R. Walker, D. M. Freye, R. K. W. Haselwimmer and G. G. Lonzarich: Nature **394** (1998) 39.
4) S. Nakatsuji, K. Kuga, Y. Machida, T. Tayama, T. Sakakibara, Y. Karaki, H. Ishimoto, S. Yonezawa, Y. Maeno, E. Pearson, G. G. Lonzarich, L. Balicas, H. Lee and Z. Fisk: Nature Phys. **4** (2008) 603.
5) R. Settai, T. Takeuchi and Y. Ōnuki: J. Phys. Soc. Jpn. **76** (2007) 051003.
6) J. Flouquet and H. Harima: arXiv:0910.3110.
7) J. Flouquet and H. Harima: *Kotai Butsuri* (Solid State Physics) **47** (2012) 47 [in Japanese].
8) A. Ochiai, T. Suzuki and T. Kasuya: J. Phys. Soc. Jpn. 59 (1990) 4129.
9) R. Pott, W. Boksch, G. Leson, B. Politt, H. Schmidt, A. Freimuth, K. Keulerz, J. Langen, G. Neumann, F. Oster, J. Röhler, U. Walter, P. Weidner and D. Wohlleben: Phys. Rev. Lett. **54** (1985) 481.
10) P. Bonville, J. Hammann, J. A. Hodges, P. Imbert and G. J. Jéhanno: Phys. Rev. Lett. **57** (1986) 2733.
11) A. Landelli, G. L. Olcese and A. Palenzona: J. Less-Cmmon Met. **76** (1980) 317.
12) A. Mitsuda, K. Yamada, M. Sugishima and H. Wada, Physica B **404** (2009) 3002.
13) T. Hasegawa, N. Ogita, M. Sugishima, A. Mitsuda, H. Wada and M. Udagawa, J. Phys.: Conf. Ser. **273** (2011) 012030.
14) Y. Tokiwa, S. Grünheit, H. S. Jeevan, C. Stingl and P. Gegenwart: J. Phys.: Conf. Ser. **273** (2011) 012062.
15) M. Sugishima, K. Yamada, A. Mitsuda, H. Wada, K. Matsubayashi, Y. Uwatoko, K. Suga and K. Kindo: J. Phys.: Condens. Matter **22** (2010) 375601.
16) P. C. Canfield and Z. Fisk: Phil. Mag. B **65** (1992) 1117.
17) N. Tateiwa and Y. Haga: Rev. Sci. Instrum **80** (2009) 123901.
18) S. Klotz, K. Takemura, Th. Strässle and Th. Hansen: J. Phys.: Condens. Matter **24** (2012) 325103.
19) G. Knebel, D. Braithwaite, P. C. Canfield, G. Lapertot and J. Flouquet: Phys. Rev. B **65** (2001) 024425.
20) S. Kawasaki, M. Yashima, Y. Kitaoka, K. Takeda, K. Shimizu, Y. Oishi, M. Takata, T. C. Kobayashi, H. Harima, S. Araki, H. Shishido, R. Settai and Y. Ōnuki: Phys. Rev. B **77** (2008) 064508.
21) K. Miyake and H. Maebashi: J. Phys. Soc. Jpn. **71** (2002) 1007.
22) R. Takahashi, T. Honda, A. Miyake, T. Kagayama, K. Shimizu, T. Ebihara, T. Kimura and Y. Wakabayashi: arXiv:1303.4831.
23) U. Walter and D. Wohlleben: Phys. Rev. B **35** (1987) 3576.
24) K. Iwasa, M. Kohgi, N. Nakajima, R. Yoshitake Y. Hisazaki, H. Osumi, K. Tajima, N. Wakabayashi, Y. Haga, A. Ochiai, T. Suzuki and A. Uesawa: J. Magn. Magn. Mater. **177-181** (1998) 393.
25) U. Staub, B. D. Patterson, C. Schulze-Briese, F. Fauth, M. Shi, L. Soderholm, G. B. M. Vaughan and A. Ochiai: Europhys. Lett., **53** (2001) 72.
26) Y. Muro, K. Yamane, M.-S. Kim, T. Takanatake, C. Godart and P. Rogl: J. Phys. Soc. Jpn. **72**(2003) 1745.
27) M. Rams, K. Królas, P. Bonville, E. Alleno, C. Godart, D. Kaczorowski and P. Canepa: Phys. Rev. B **56** (1997) 3690.
28) P. Bonville, C. Godart, E. Alleno, F. Takahashi, E. Matsuoka and M. Ishikawa: J. Phys.: Condens. Matter **15** (2003) L263.
29) T. M. Rice and K. Ueda: Phys. Rev. B **34** (1986) 6420.
30) D. Malterre, M. Grioni and Y. Baer: Adv. Phys. **45** (1996) 299.
31) J. Flouquet, A. Barla, R. Boursier, J. Derr and G. Knebel: J. Phys. Soc. Jpn. **74** (2005) 178.
32) P. Bonville, A. Ochiai, T. Suzuki and E. Vincent: J. Phys. I France **4** (1994) 595.
33) T. Park, V. A. Sidorov, J. L. Sarrao and J. D. Thompson: Phys. Rev. Lett. **96** (2006) 046405.
34) A. V. Goltsev and M. M. Abd-Elmeguid: J. Phys.: Condens. Matter **17** (2005) S813.
35) K. Alami-Yadri, H. Wilhelm and D. Jaccard: Eur. Phys. J. B **6** (1998) 5.